

## Stimulated Parametric Down-Conversion with Vector Vortex Beams

N. Rubiano da Silva<sup>1</sup>, A.G. de Oliveira<sup>1</sup>, M.F.Z. Arruda,<sup>1,2</sup> R. Medeiros de Araújo,<sup>1</sup>  
W.C. Soares,<sup>3</sup> S.P. Walborn,<sup>4,5,6</sup> R.M. Gomes,<sup>7</sup> and P.H. Souto Ribeiro<sup>1,\*</sup>

<sup>1</sup>*Departamento de Física, Universidade Federal de Santa Catarina, Florianópolis, SC CEP 88040-900, Brazil*

<sup>2</sup>*Instituto Federal de Mato Grosso, Sorriso, MT CEP 78890-000, Brazil*


<sup>3</sup>*Núcleo de Ciências Exatas – NCEX, Universidade Federal de Alagoas, Arapiraca, AL CEP 57309-005, Brazil*

<sup>4</sup>*Instituto de Física, Universidade Federal do Rio de Janeiro, Caixa Postal 68528, Rio de Janeiro, RJ 21941-972, Brazil*

<sup>5</sup>*Departamento de Física, Universidad de Concepción, 160-C Concepción, Chile*

<sup>6</sup>*ANID – Millennium Science Initiative Program – Millennium Institute for Research in Optics, Universidad de Concepción, 160-C Concepción, Chile*

<sup>7</sup>*Instituto de Física, Universidade Federal de Goiás, Goiânia, GO CEP 74690-900, Brazil*

 (Received 28 October 2020; revised 15 December 2020; accepted 5 January 2021; published 17 February 2021)

A vector vortex beam presents local polarization states that are spatially modulated in the plane transverse to propagation. By employing a two-crystal-sandwich source allowing for nonlinear interactions between input fields of any polarization, we analyze experimentally the process of stimulated parametric down-conversion and observe unique effects when the pump and seed fields are vector vortex beams. We reconstruct the transverse polarization pattern of the generated idler beam by Stokes polarimetry. The experimental results obtained are in good qualitative agreement with theory and exhibit manifold polarization transverse distributions for different combinations of pump and seed vector vortex beams, which may find applications in both classical and quantum optics.

DOI: [10.1103/PhysRevApplied.15.024039](https://doi.org/10.1103/PhysRevApplied.15.024039)

### I. INTRODUCTION

Vector beams are structured light beams that present a polarization state that varies in the plane transverse to the propagation axis [1–3]. A particular class is that of paraxial beams with cylindrical symmetry in both intensity and polarization transverse distributions and a singularity along the beam axis, the so-called vector vortex beams [3, 4]. These are very interesting physical systems that can be interpreted as a classical analog of the entangled Bell states [5], since polarization and transverse (i.e., spin and orbit) degrees of freedom are nonseparable [6,7]. These hybrid entangled states can be exploited, for instance, in kinematic sensing of fast-moving objects [8], and in high-dimensional encoding and transmission of information [9]. Generally, there has been a growing number of proposals for practical applications in communication [10] and precision measurement schemes [11], among other fields [12–14].

There has also been an increasing interest in the research for unusual types of structured beams [3] and their interaction with matter [15], for instance, to manipulate atoms [16]. By using vector beams in nonlinear optical processes in general, phenomena, such as optical phase

conjugation [17], gain different perspectives [18,19]. More specifically, second-harmonic generation induced by vector beams has been uncovering the role played by the spin-orbit interaction between light and nonlinear media [20,21].

Here, we study the physical consequences of using vector vortex beams in the nonlinear process of stimulated parametric down-conversion (StimPDC) [22]. Phase-matching conditions in parametric down-conversion are polarization dependent for most nonlinear optical materials and for this reason it is necessary to use an adequate nonlinear source that allows for the complete interaction of structured beams. To this end, we use the two-crystal-sandwich source introduced for the realization of a high-intensity source of polarization-entangled photon pairs in the regime of spontaneous down-conversion [23]. Pumping and seeding this type of source with vector vortex beams generates a third beam—the idler, which is also a structured beam, and whose properties depend explicitly on those of the pump and the seed. We measure its transverse intensity profile and perform transverse-position-dependent polarization tomography, which allows for the complete description of the beam. We find good qualitative agreement between our measurements and the predictions of a recently introduced theory [24]. We also find that some combinations of pump and seed vector

\*p.h.s.ribeiro@ufsc.br

vortex beams generate an idler beam that is a superposition of paraxial beams with different Gouy phases, resulting in diffraction effects that change both the transverse intensity and the polarization profiles. The results of this investigation with stimulated down-conversion are also valid in the context of spontaneous parametric down-conversion, given that the mode coupling and phase-matching conditions are the same for both processes [25]. They are also useful for applications in which frequency conversion of vector vortex beams is necessary and have potential utility in simulation of dynamical physical systems using light beams.

## II. EXPERIMENTAL SETUP

The experimental scheme used to study the StimPDC process with pump and/or seed beams prepared as vector vortex beams is shown in Fig. 1(a). A 405-nm cw diode laser is used as the pump beam and a 780-nm cw diode laser is used as the seed (signal) beam. Both beams have optical power around 40 mW. They are collimated using a telescope, such that their diameters are about 1.0 mm throughout the interaction region. The idler beam produced in the process has a wavelength of 840 nm. Its diameter is given by the interaction region where pump and seed overlap, and under proper alignment it is also nearly 1.0 mm. The down-conversion source is formed by two beta barium borate (BBO) crystals cut for type-I phase-matching interaction. They are placed close together with a relative rotation of  $90^\circ$  (about the optical axis), so that one

crystal is pumped with horizontal ( $H$ ) polarization and generates down-converted light with vertical ( $V$ ) polarization, while the other crystal is pumped with  $V$  polarization and emits in  $H$  polarization modes [see Fig. 1(b)]. This is often referred to as the two-crystal-sandwich source, which was conceived to generate entangled photon states with the polarization degree of freedom [23].

In order to achieve temporal overlap between the idler polarization modes produced in the two different crystals, we use pump and seed lasers having coherence lengths larger than the total length of the two-crystal source. We use 2-mm-thick crystals, so that the coherence lengths should be larger than 4 mm, which is easily attainable with commercial diode lasers. Temporal overlap between modes produced in different crystals can be achieved by other means when the lasers have short coherence lengths or are pulsed [26,27]. The crystal length is also much shorter than the Rayleigh length of pump and seed beams, so that the Gouy phases of both beams can be assumed to be constant within the interaction volume. Relaxing this condition can give rise to a varying phase difference between horizontal and vertical components of the idler inside the crystal. The optical alignment is achieved by measuring coincidence counts between signal and idler photons produced by spontaneous PDC (seed turned off) and detected with single-photon counting modules (SPCM) with 10-nm bandwidth interference filters having central wavelengths of 780 and 840 nm. Once the coincidence alignment is obtained, the path of the 780-nm signal beam is marked with pinholes and the seed

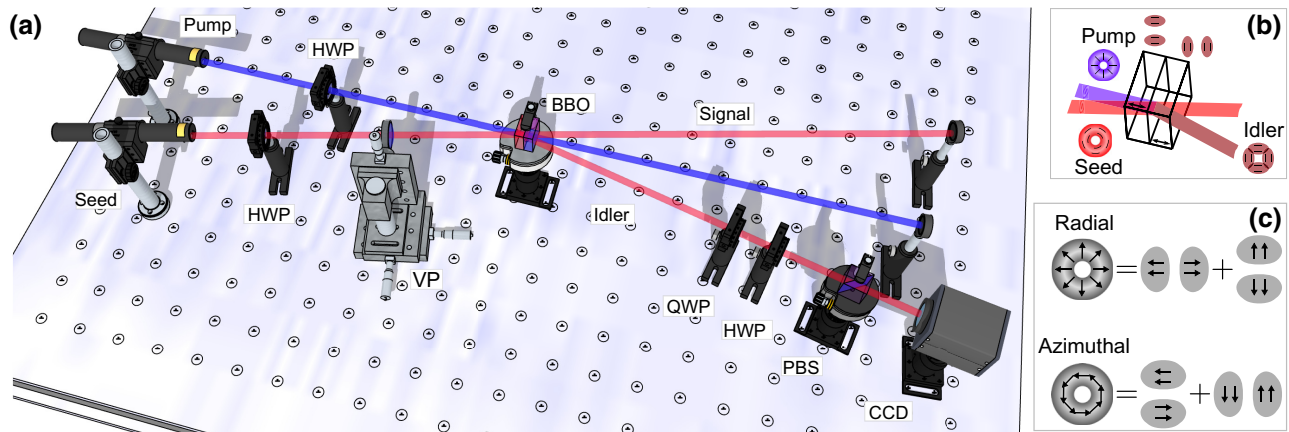


FIG. 1. StimPDC with vector beams. (a) Experimental setup. Two cw-laser beams (pump and seed) are collimated using a telescope (not shown), and then prepared in polarization states by using half-wave plates (HWPs) and vortex plates (VPs, shown here only for the seed beam). An enhanced idler beam is generated by StimPDC when the two beams are incident on a pair of nonlinear crystals (BBO). All polarization components of pump and seed beams participate in the process due to the use of the two-crystal-sandwich source. The polarization state of the idler beam is measured in the transverse plane by the combination of a polarization tomographic setup (quarter-wave plate (QWP), HWP, and polarizing beam splitter (PBS)) and a CCD camera. (b) The sandwich source: two identical type-I BBO crystals placed with a relative rotation of  $90^\circ$  (as indicated by the arrows), each contributing coherently to StimPDC in the transverse portions of the pump and seed vector beams. Here, the pump and seed are displayed with radial and azimuthal polarization profiles, respectively. The polarization line is indicated by black, solid strokes. (c) Decomposition of radial and azimuthal modes in horizontal and vertical polarization components.

laser is injected through the source collinearly with it. This causes the intensity of the idler to increase enough to replace the SPCM detectors with a conventional CCD camera.

Pump and seed beams are prepared in vector vortex modes using commercial vortex plates (Thorlabs). We prepare beams with topological charges  $m = 1$  [radial and azimuthal polarization distributions, see Fig. 1(c)] and  $m = 2$ . For each combination of pump and seed beam, the intensity and polarization pattern of the idler beam is measured by Stokes polarimetry [28] in the following way. First, we record a set of six images on a CCD camera (Thorlabs CS2100M-USB Quantalux) combined with a 10-nm-bandwidth, 840-nm-centered bandpass interference filter, when imaging the idler, and neutral density filters when imaging pump and seed. Each image corresponds to a projection onto horizontal-vertical ( $H$ - $V$ ), diagonal-antidiagonal ( $D$ - $A$ ), and right-circular-left-circular ( $R$ - $L$ ) polarization basis, realized with a QWP, a HWP, and a PBS. The exposure time is 7.8 s for each idler-beam image, and 100 ms for seed and pump beam images. The images are then used to compute the Stokes parameters at each point [29], and then reconstruct the spatial distribution of intensity and polarization profile of the light beams. In order to reduce experimental errors in the reconstruction, we replace the value in each pixel by the average intensity within a square of  $20 \times 20$  pixels around it, and use these smoothed tomographic projections for computing the maps of Stokes parameters. The polarization states represented in the reconstructed patterns do not account for the corresponding intensity at the given point of the spatial profile. Therefore, one may have a polarization state displayed in a point where the intensity would be ideally zero.

### III. QUANTUM-OPTICAL DESCRIPTION

The vortex plates generate vector beams with rotational symmetry, also known as cylindrical vortex beams [4,30]. The electric field of such a beam can be represented as a superposition of two counter-rotating circularly polarized fields [2,31]:

$$\mathbf{E}(r, \varphi) = A_m(r) \left[ e^{-i(m\varphi+\alpha)} (\hat{\mathbf{x}} + i\hat{\mathbf{y}}) + e^{i(m\varphi+\alpha)} (\hat{\mathbf{x}} - i\hat{\mathbf{y}}) \right], \quad (1)$$

where  $A_m(r)$  is the complex-amplitude transverse profile of a Laguerre-Gaussian mode of radial order  $p = 0$  and azimuthal order  $m$ , apart from the term  $e^{-im\varphi}$ . The angle  $\alpha$  is the angle between the polarization of the input beam and the “main” fast axis of the vortex plate.  $r$  and  $\varphi$  are the usual cylindrical coordinates at the transverse plane, and  $\hat{\mathbf{x}}$  and  $\hat{\mathbf{y}}$  are the Cartesian unit vectors associated with horizontal and vertical polarizations, respectively.

We can rewrite Eq. (1) as

$$\mathbf{E}(r, \varphi) = 2A_m(r) \left[ \cos(m\varphi + \alpha) \hat{\mathbf{x}} + \sin(m\varphi + \alpha) \hat{\mathbf{y}} \right], \quad (2)$$

allowing for the analytical description of the vortex beams intensity ( $|\mathbf{E}|^2$ ) and polarization ( $\mathbf{E}$ ) transverse profiles. In our experimental setup, we can generate pump and seed beams of various profiles. Linearly polarized Gaussian beams ( $m = 0$ ) are generated using only the HWP. Radial ( $m = 1, \alpha = 0$ ) and azimuthal ( $m = 1, \alpha = \pi/2$ ) beams are created with the use of a HWP and a vortex plate [see polarization patterns in Fig. 1(c)]. A hybrid vector beam [32], which is a more complex beam containing linear, elliptic, and circular polarization states, can be generated using a QWP and a vortex plate. The electric field of such a hybrid field is obtained from Eq. (2) by operating on it with the appropriate Jones matrix.

The stimulated idler beam will inherit its polarization properties from the coupling between the pump and seed fields. As shown in Ref. [24], when projected onto a polarization state given by

$$|\theta, \phi\rangle = \cos \frac{\theta}{2} |H\rangle + e^{i\phi} \sin \frac{\theta}{2} |V\rangle, \quad (3)$$

the intensity of the stimulated idler field at a position  $\mathbf{r}$ , within the paraxial approximation can be written as

$$\begin{aligned} I_{\theta, \phi}^{\text{stim}}(\mathbf{r}) &= \frac{1}{2} \cos^2 \frac{\theta}{2} |\mathcal{F}_H(\boldsymbol{\rho})|^2 + \frac{1}{2} \sin^2 \frac{\theta}{2} |\mathcal{F}_V(\boldsymbol{\rho})|^2 \\ &\quad + \frac{e^{i\phi}}{4} \sin \theta \mathcal{F}_V^*(\boldsymbol{\rho}) \mathcal{F}_H(\boldsymbol{\rho}) \\ &\quad + \frac{e^{-i\phi}}{4} \sin \theta \mathcal{F}_H^*(\boldsymbol{\rho}) \mathcal{F}_V(\boldsymbol{\rho}), \end{aligned} \quad (4)$$

where  $\boldsymbol{\rho} = (x, y)$  gives the transverse position coordinates at the detection plane. The function  $\mathcal{F}_j(\boldsymbol{\rho})$  describes the idler field of wave number  $k_i$  in the polarization  $j = H, V$ , after a propagation distance  $z$ :

$$\mathcal{F}_j(\boldsymbol{\rho}) = \int d\boldsymbol{\rho}' \mathcal{W}_j(\boldsymbol{\rho}') \mathcal{U}_j^*(\boldsymbol{\rho}') \times \exp \left[ i|\boldsymbol{\rho} - \boldsymbol{\rho}'|^2 \frac{k_i}{2z} \right], \quad (5)$$

where  $\mathcal{W}_j(\boldsymbol{\rho})$ ,  $\mathcal{U}_j^*(\boldsymbol{\rho})$  are the components of the transverse-mode profiles of the pump beam and seed beam, respectively, and  $\bar{j}$  is the polarization direction orthogonal to  $j$ . The field profiles are defined in Eq. (2). Therefore,

$$\mathcal{W}_j(\boldsymbol{\rho}) \mathcal{U}_j^*(\boldsymbol{\rho}) = 4A_p(r) A_s^*(r) f_j(l\varphi + \alpha) f_{\bar{j}}(m\varphi + \beta), \quad (6)$$

where the index  $p$  and the parameters  $l$  and  $\alpha$  ( $s$ ,  $m$ , and  $\beta$ ) relate to the pump (seed) beam; while  $f_H(t) = \cos(t)$  and  $f_V(t) = \sin(t)$ .

### IV. StimPDC OF VECTOR BEAMS: RESULTS AND DISCUSSION

Equations (5) and (6) can be used in Eq. (4) to compute the intensity of any polarization projection of the

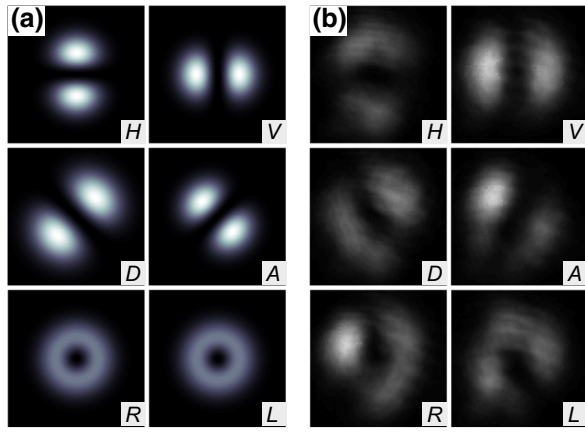


FIG. 2. Tomographic projections of idler beam in StimPDC, when pump is a radial mode and seed has diagonal polarization. Simulated (a) and experimental (b) projections of the idler beam in the  $H$ - $V$ ,  $D$ - $A$ , and  $R$ - $L$  bases.

idler field at the detection plane. To illustrate this capability, Fig. 2 displays six projections of the idler beam for a radially polarized pump beam and a diagonally polarized seed beam, obtained by both the simulation and the measurement. There is clearly a good qualitative agreement between the theoretically predicted and the observed projections, which prevails for all the cases we investigate here. We note that, even though the results above are derived for cylindrical vortex pump and seed beams, they are general enough to describe the case of linearly polarized pump and/or seed Gaussian beam, since such beams can be obtained from Eq. (2) by setting  $m = 0$ .

We test StimPDC for a variety of different combinations of pump and seed beams, as we now describe. Let us start with a linearly polarized pump and a cylindrical vector seed beam, extending the observations of Ref. [19]. Figure 3 (central column) shows the measured intensity profile and the tomographically reconstructed polarization of the idler beam, for combinations of diagonally-antidiagonally polarized pump and radially-azimuthally polarized seed beam [radial and azimuthal modes are illustrated in Fig. 1(c)]. Interchanging the pump and seed polarization profiles brings up analogous idler polarizations. Figure 3 (right column) displays the observed idler profiles obtained using radially-azimuthally polarized pump and diagonally-antidiagonally polarized seed.

The polarization profiles of the idler beam have some interesting features. First, it reproduces the seed polarization state when the pump is diagonal, while being transformed relative to the seed when the pump is antidiagonal. These results corroborate the interpretation of thin-crystal PDC in terms of phase conjugation, observed in Ref. [19] and described using quantum optics tools in Ref. [24]. Secondly, there are four different cylindrical vector modes that can be generated in StimPDC using

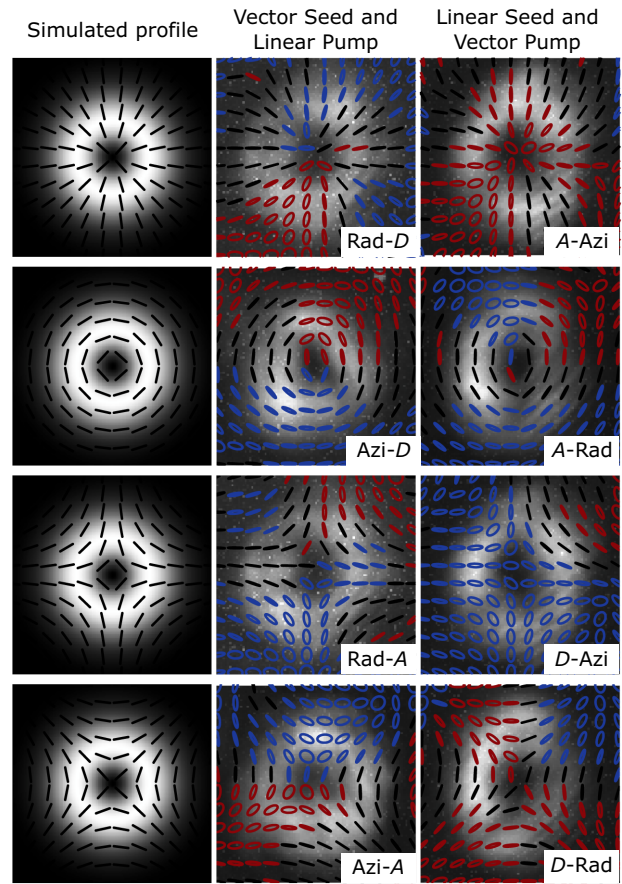


FIG. 3. StimPDC combining a cylindrical vector beam and a linearly polarized beam. Simulated (left column) and measured (central and right columns) transverse profiles of idler beam. The intensity is shown in the gray colorscale. The state of polarization is indicated by the black lines (linear polarization), and colored ellipses (red for right and blue for left handedness, respectively).

our two-crystal source and a combination of a radially-azimuthally polarized beam and a linearly polarized one. Indeed, the output idler beam can also be described by Eq. (2), with the parameters  $\alpha$  and  $m$  being determined by the polarization states of the input pump and seed beams. For instance, an azimuthally polarized pump and a diagonally polarized seed (right panel at the third row in Fig. 3) produce a cylindrical vector beam with  $\alpha = 0$  and  $m = -1$ , an antivortex mode [2]. Lastly, there is some small ellipticity in parts of the observed idler profile, which cannot be explained in the ideal process (simulation). We understand that these stem from (i) small deviations from optimum phase-matching conditions; (ii) relative crystal rotation not exactly at  $90^\circ$ ; (iii) imperfections in tomographic setup, such as imperfect waveplates; and (iv) pump and seed are not collinear before the StimPDC source in the experiment, while taken as such in the simulation, which can lead to different birefringence effects between beams as they propagate through the crystals.

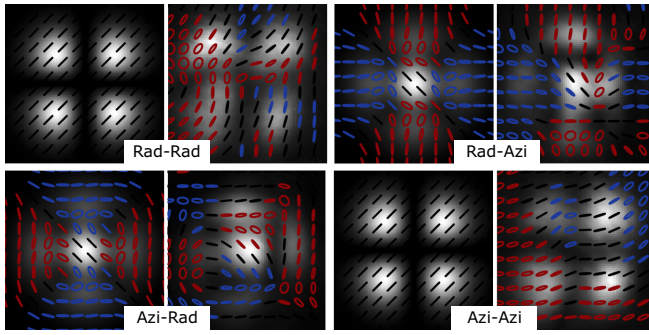


FIG. 4. StimPDC using vector vortex beams for both pump and seed. Simulated (left) and measured (right) transverse profiles of idler beam. Seed and pump polarization states are labeled. The gray colorscale represents the intensity, while the state of polarization is indicated by the black lines (linear polarization), and colored ellipses (red for right and blue for left handedness, respectively).

More interesting effects arise when using vector vortex beams for both pump and seed in two-crystal StimPDC. By using combinations of radial and azimuthal beams, the idler will have more distinguishing features, as shown in Fig. 4. The idler beam presents either a simple polarization distribution and a complex intensity profile (when pump and seed are similar, i.e., radial-radial or azimuthal-azimuthal) or complex polarization and intensity distributions (when pump and seed are different). It is worthwhile to note that the intensity profile for similar pump and seed beams corresponds to a two-dimensional Hermite-Gaussian distribution of order 2 (specifically, the  $HG_{11}$  mode), while the input beams are Laguerre-Gaussian modes of order 1. Accordingly, the so-obtained idler field exhibits a beamlike propagation behavior, with diffraction effects on the intensity and fixed polarization profile. When different pump and seed beams are combined, however, the idler beam at the crystal evolves upon propagation from a petal-like intensity profile with no intensity in the center [schematically shown in Fig. 1(b)] to the shape in the top right and bottom left panels of Fig. 4. Moreover, the polarization profile evolves from homogeneously linear to a more complex one, containing even circularly polarized regions.

We explore further the power of this kind of source for generating even more intricate polarization states, by pumping and/or seeding it with higher-order cylindrical vector beams and hybrid vector beams. Figure 5 displays the idler beams obtained by using a cylindrical vector beam of order  $m = 2$  as a pump [see Fig. 5(a)], and different seed beams. Once again, a linearly polarized seed results in idler beams, which are cylindrical vector modes [Fig. 5(b)], and a seed beam of the same order and polarization distribution as the pump leads to an idler with simple, petal-like intensity distribution and homogeneous linear polarization [Fig. 5(d)]. As for the intermediate combination, i.e., a

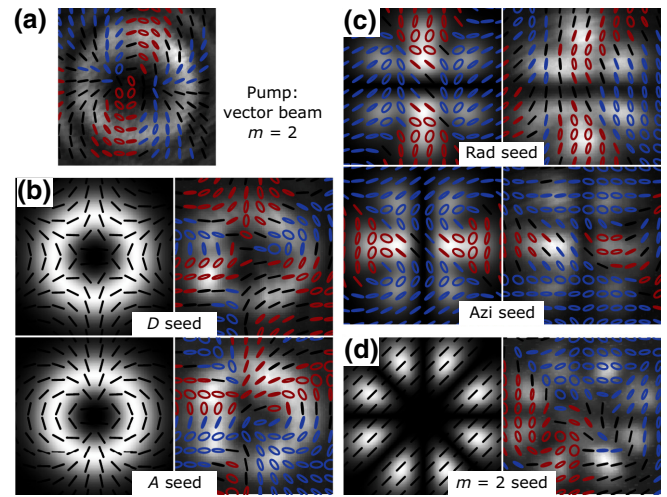


FIG. 5. StimPDC with a pump vector vortex beam of order  $m = 2$  and different seed configurations. (a) Pump beam of order  $m = 2$ . (b)–(d) Simulated (left panels) and measured (right panels) transverse profiles of idler beams obtained using (b) linearly polarized seed, (c) seed of order  $m = 1$ , and (d) seed of order  $m = 2$ . Gray scale, intensity; black lines, linear polarization; red (blue) ellipses, polarization with right (left) handedness.

cylindrical vector seed beam of order 1, a petal-like intensity profile containing circular polarization states is formed at the detector plane. The circularity here and in the case of radial-azimuthal pump and seed derives from (i) the fact that each orthogonal component of the idler field is a superposition of different spatial modes, and (ii) the fact that modes of different order have distinct Gouy phases. As a result, the relative phase between the orthogonal components is a function of the propagation distance. A similar effect, the rotation of polarization profiles upon propagation within the Rayleigh range, was previously reported for Poincaré beams, another class of vector beams [33,34]. In that case, the vector beams are described as a superposition of Laguerre-Gaussian states with different orders [e.g., given by Eq. (1) with different orders for right and left circular polarized fields].

Of course, a straightforward way to obtain elliptical states of polarization in the idler beam is to have them already at the seed beam. Here, we create such inhomogeneously polarized seed beams by sending the radial-azimuthal beam through a QWP. The hybrid vector beam profiles are shown in Fig. 6(a), and the idler beams generated by combining them with a linearly or radially polarized pump are displayed in Figs. 6(b)–6(d). Even for the complex seed polarization profile, the idler beam obtained by using an antidiagonally polarized beam as a pump is very similar to it, in resemblance to the effects depicted in Fig. 3 (the two lower central panels). As for a radially polarized pump beam, very intricate polarization profiles are generated [lower panels of Figs. 6(b)

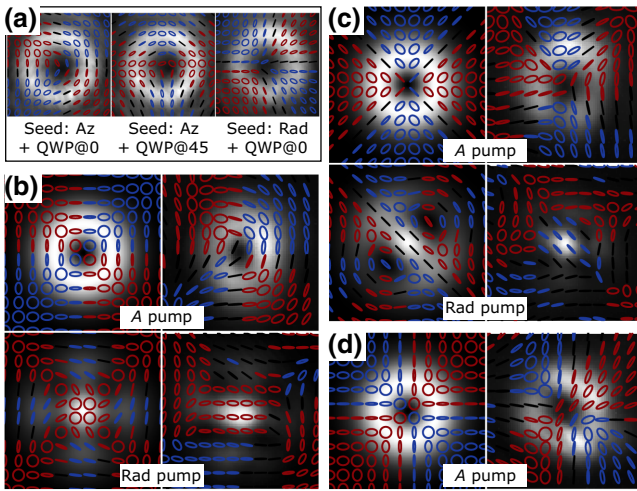


FIG. 6. StimPDC with a hybrid vector beam as the seed, and the pump with linear polarization or vector-vortex-beam configurations. (a) Seed profiles. (b)–(d) Simulated (left panels) and measured (right panels) transverse profiles of idler beam using as a seed (b) the beam at the left panel of (a), (c) the beam at the central panel of (a), (d) the beam at the right panel of (a). Gray scale, intensity; black lines, linear polarization; red (blue) ellipses, polarization with right (left) handedness.

and 6(c)]. Note that they differ strongly from the ones obtained when using cylindrical vector beams as pump and seed (Fig. 4), which contain only linear polarization states. Specifically, the combination of radial modes for both seed and pump, which previously resulted in an idler beam mode of petal-like intensity distribution and homogeneous diagonal polarization (cf. upper left panel of Fig. 4), shows now a very complex intensity and polarization distribution [lower panel of Fig. 6(c)]. We attribute such behavior to a combination of the circularity resulting from different spatial modes in each orthogonal component of the electric field, as observed before, and from the intrinsic elliptical states of polarization in the idler beam, inherited from the seed.

## V. CONCLUSIONS

In conclusion, we perform stimulated parametric down-conversion using a two-crystal-sandwich source being pumped and seeded with combinations of vector vortex beams (up to topological charge  $m = 2$ ). We measure the idler beam generated in the process and perform position-dependent polarization tomography, which results in transverse intensity and polarization maps. The experimental patterns are in good qualitative agreement with theory. Among the combinations used, we find that, when the pump (seed) beam is prepared in a linear diagonal or antidiagonal state and the seed (pump) is prepared as a vector vortex beam, there is essentially the transfer of the vector vortex structure to the generated idler beam. When

both pump and seed are vector vortex beams, we observe two very distinct outcomes. In the case of equal polarization patterns for both beams, the resulting idler is not a vector beam anymore, having a homogeneous linear polarization; and in the case of combining different polarization patterns, the idler is not even a Gaussian mode anymore. This last case presents the interesting feature of diffracting and displaying a dynamic polarization structure. We also test interactions between a hybrid vector beam as the seed, and linearly polarized Gaussian beams and vector vortex beams as the pump. The results are similar to the cases where the seed is a vector vortex beam containing only linear polarization states, with the difference being the presence of elliptically polarized components in the idler pattern.

Our results show that stimulated parametric down-conversion with the two-crystal-sandwich source is a reliable process to realize and study the interaction between structured beams. We note that the inverse process, second-harmonic generation with vector beams, has been recently investigated [35,36], and is also useful in this kind of study. Together with the wavelength tuning provided by the down-conversion process, the flexibility to generate various intensity and polarization distributions with our experimental setup can be used in all applications of vector vortex beams. We also believe that this scheme can be useful for the study or emulation of interactions and dynamics of qubits prepared in Bell states.

## ACKNOWLEDGMENTS

The authors would like to thank the Brazilian Agencies, Conselho Nacional de Desenvolvimento Tecnológico (CNPq), Fundação Carlos Chagas Filho de Amparo à Pesquisa do Estado do Rio de Janeiro (FAPERJ), Fundação de Amparo à Pesquisa e Inovação do Estado de Santa Catarina (FAPESC), Fundação de Amparo à Pesquisa do Estado de Goiás (FAPEG), Fundação de Amparo à Pesquisa do Estado de Alagoas (FAPEAL) and the Brazilian National Institute of Science and Technology of Quantum Information (INCT/IQ). This study was financed in part by the Coordenação de Aperfeiçoamento de Pessoal de Nível Superior – Brasil (CAPES) – Finance Code 001 and via the Programa Nacional de Cooperação Acadêmica. SPW received support from the Fondo Nacional de Desarrollo Científico y Tecnológico (FONDECYT) (Grant No. 1200266) and the ANID – Millennium Science Initiative Program – ICN17\_012.

- 
- [1] F. Gori, Polarization basis for vortex beams, *J. Opt. Soc. Am. A* **18**, 1612 (2001).
  - [2] C. Maurer, A. Jesacher, S. Fürhapter, S. Bernet, and M. Ritsch-Marte, Tailoring of arbitrary optical vector beams, *New J. Phys.* **9**, 78 (2007).

- [3] H. Rubinsztein-Dunlop *et al.*, Roadmap on structured light, *J. Opt.* **19**, 013001 (2016).
- [4] Q. Zhan, Cylindrical vector beams: From mathematical concepts to applications, *Adv. Opt. Photonics* **1**, 1 (2009).
- [5] S. J. Freedman and J. F. Clauser, Experimental Test of Local Hidden-Variable Theories, *Phys. Rev. Lett.* **28**, 938 (1972).
- [6] C. V. S. Borges, M. Hor-Meyll, J. A. O. Huguenin, and A. Z. Khoury, Bell-like inequality for the spin-orbit separability of a laser beam, *Phys. Rev. A* **82**, 033833 (2010).
- [7] A. Holleczek, A. Aiello, C. Gabriel, C. Marquardt, and G. Leuchs, Classical and quantum properties of cylindrically polarized states of light, *Opt. Express* **19**, 9714 (2011).
- [8] S. Berg-Johansen, F. Töppel, B. Stiller, P. Banzer, M. Ornigotti, E. Giacobino, G. Leuchs, A. Aiello, and C. Marquardt, Classically entangled optical beams for high-speed kinematic sensing, *Optica* **2**, 864 (2015).
- [9] Y. Zhao and J. Wang, High-base vector beam encoding/decoding for visible-light communications, *Opt. Lett.* **40**, 4843 (2015).
- [10] V. D'Ambrosio, E. Nagali, S. P. Walborn, L. Aolita, S. Slussarenko, L. Marrucci, and F. Sciarrino, Complete experimental toolbox for alignment-free quantum communication, *Nat. Commun.* **3**, 961 (2012).
- [11] V. D'Ambrosio, N. Spagnolo, L. Del Re, S. Slussarenko, Y. Li, L. C. Kwek, L. Marrucci, S. P. Walborn, L. Aolita, and F. Sciarrino, Photonic polarization gears for ultra-sensitive angular measurements, *Nat. Commun.* **4**, 2432 (2013).
- [12] V. D'Ambrosio, G. Carvacho, F. Graffitti, C. Vitelli, B. Piccirillo, L. Marrucci, and F. Sciarrino, Entangled vector vortex beams, *Phys. Rev. A* **94**, 030304(R) (2016).
- [13] M. Yoshida, Y. Kozawa, and S. Sato, Subtraction imaging by the combination of higher-order vector beams for enhanced spatial resolution, *Opt. Lett.* **44**, 883 (2019).
- [14] I. Gianani, A. Suprano, T. Giordani, N. Spagnolo, F. Sciarrino, D. Gorpas, V. Ntziachristos, K. Pinker, N. Biton, J. Kupferman, and S. Armon, Transmission of vector vortex beams in dispersive media, *Adv. Photonics* **2**, 036003 (2020).
- [15] J. Wang, F. Castellucci, and S. Franke-Arnold, Vectorial light-matter interaction: Exploring spatially structured complex light fields, *AVS Quantum Sci.* **2**, 031702 (2020).
- [16] M. Babiker, D. L. Andrews, and V. E. Lembessis, Atoms in complex twisted light, *J. Opt.* **21**, 013001 (2018).
- [17] R. A. Fisher, ed., *Optical Phase Conjugation* (Academic Press, San Diego, 1983).
- [18] S.-X. Qian, Y. Li, L.-J. Kong, C. Tu, and H.-T. Wang, Phase conjugation of vector fields by degenerate four-wave mixing in a Fe-doped LiNbO<sub>3</sub>, *Opt. Lett.* **39**, 4907 (2014).
- [19] A. G. de Oliveira, M. F. Z. Arruda, W. C. Soares, S. P. Walborn, R. M. Gomes, R. Medeiros de Araújo, and P. H. Souto Ribeiro, Real-time phase conjugation of vector vortex beams, *ACS Photonics* **7**, 249 (2020).
- [20] H.-J. Wu, H.-R. Yang, C. Rosales-Guzmán, W. Gao, B.-S. Shi, and Z.-H. Zhu, Vectorial nonlinear optics: Type-II second-harmonic generation driven by spin-orbit-coupled fields, *Phys. Rev. A* **100**, 053840 (2019).
- [21] Y. Tang, K. Li, X. Zhang, J. Deng, G. Li, and E. Brasselet, Harmonic spin-orbit angular momentum cascade in nonlinear optical crystals, *Nat. Photonics* **14**, 658 (2020).
- [22] L. J. Wang, X. Y. Zou, and L. Mandel, Observation of induced coherence in two-photon downconversion, *J. Opt. Soc. Am. B* **8**, 978 (1991).
- [23] P. G. Kwiat, E. Waks, A. G. White, I. Appelbaum, and P. H. Eberhard, Ultrabright source of polarization-entangled photons, *Phys. Rev. A* **60**, R773 (1999).
- [24] A. G. de Oliveira, N. Rubiano da Silva, R. Medeiros de Araújo, P. H. Souto Ribeiro, and S. P. Walborn, Quantum Optical Description of Phase Conjugation of Vector Vortex Beams in Stimulated Parametric Down-Conversion, *Phys. Rev. Appl.* **14**, 024048 (2020).
- [25] M. F. Z. Arruda, W. C. Soares, S. P. Walborn, D. S. Tasca, A. Kanaan, R. Medeiros de Araújo, and P. H. Souto Ribeiro, Klyshko's advanced-wave picture in stimulated parametric down-conversion with a spatially structured pump beam, *Phys. Rev. A* **98**, 023850 (2018).
- [26] J. B. Altepeter, E. R. Jeffrey, and P. G. Kwiat, Phase-compensated ultra-bright source of entangled photons, *Opt. Express* **13**, 8951 (2005).
- [27] R. Rangarajan, M. Goggin, and P. Kwiat, Optimizing type-I polarization-entangled photons, *Opt. Express* **17**, 18920 (2009).
- [28] K. Singh, N. Tabebordbar, A. Forbes, and A. Dudley, Digital stokes polarimetry and its application to structured light: Tutorial, *J. Opt. Soc. Am. A* **37**, C33 (2020).
- [29] M. Born and E. Wolf, *Principles of Optics* (Pergamon Press, Kronberg, 1989), 6th ed.
- [30] K. S. Youngworth and T. G. Brown, Focusing of high numerical aperture cylindrical-vector beams, *Opt. Express* **7**, 77 (2000).
- [31] G. Milione, H. I. Sztul, D. A. Nolan, and R. R. Alfano, Higher-Order Poincaré Sphere, Stokes Parameters, and the Angular Momentum of Light, *Phys. Rev. Lett.* **107**, 053601 (2011).
- [32] G. Milione, H. I. Sztul, and R. R. Alfano, in *Stokes polarimetry of a hybrid vector beam from a spun elliptical core optical fiber*, edited by E. J. Galvez, D. L. Andrews, and J. Glückstad (SPIE, 2010), Proc. SPIE **7613**, 761305.
- [33] A. M. Beckley, T. G. Brown, and M. A. Alonso, Full Poincaré beams, *Opt. Express* **18**, 10777 (2010).
- [34] F. Cardano, E. Karimi, L. Marrucci, C. de Lisio, and E. Santamato, Generation and dynamics of optical beams with polarization singularities, *Opt. Express* **21**, 8815 (2013).
- [35] L. Zhang, X. Qiu, F. Li, H. Liu, X. Chen, and L. Chen, Second harmonic generation with full Poincaré beams, *Opt. Express* **26**, 11678 (2018).
- [36] H. Liu, H. Li, Y. Zheng, and X. Chen, Nonlinear frequency conversion and manipulation of vector beams, *Opt. Lett.* **43**, 5981 (2018).